High-Performance Wearable Bi2Te3-Based Thermoelectric Generator

Yubing Xing , Kechen Tang , Jiang Wang , Kai Hu , Yani Xiao , Jianan Lyv , Junhao Li , Yutian Liu , Peng Zhou , Yonggao Yan *, Dongwang Yang *

Posted Date: 26 April 2023

doi: 10.20944/preprints202304.0967.v1

Keywords: Wearable thermoelectric generator; Bi2Te3; Finite element simulation; Power generation.

High-Performance Wearable Bi_2Te_3-Based Thermoelectric Generator

Yubing Xing [1], Kechen Tang [1], Jiang Wang [1], Kai Hu [1], Yani Xiao [1], Jianan Lyu [1,2], Junhao Li [1], Yutian Liu [1], Peng Zhou [3], Yonggao Yan [1,*] and Dongwang Yang [1,*]

[1] State Key Laboratory of Advanced Technology for Materials Synthesis and Processing, Wuhan University of Technology, Wuhan 430070, China
[2] Nanostructure Research Center, Wuhan University of Technology, Wuhan 430070, China
[3] Research Center for Materials Genome Engineering, Wuhan University of Technology, Wuhan 430070, China
* Correspondence: yanyonggao@whut.edu.cn (Y.Y.); ydongwang@whut.edu.cn (D.Y.)

Abstract: Wearable thermoelectric generators (w-TEGs) convert thermal energy into electrical energy to realize self-powering of intelligent electronic devices, thus reducing the burden of battery replacement and charging, and improving the usage time and efficiency of electronic devices. Through finite element simulation, this study successfully designed high-performance thermoelectric generator and made it into wearable thermoelectric module by adopting "rigid device-flexible connection" method. It was found that higher convective heat transfer coefficient (h) on cold-end leads to larger effective temperature difference (ΔT_{eff}) and better power generation performance of device in typical wearable scenario. Meanwhile, at same h on the cold-end, longer TE leg length leads to larger ΔT_{eff} established at both ends of device, larger device output power (P_{out}) and open-circuit voltage (U_{oc}). However, when the h increases to a certain level, optimization effect of increasing TE leg length on device power generation performance will gradually diminish. For devices with fixed temperature difference between two ends, longer TE leg length leads to higher resistance of TEG, resulting in lower device P_{out} but slight increase in U_{oc}. Finally, sixteen 16×4×2 mm^2 TEGs (L=1.38 mm, W=0.6 mm) and two modules were fabricated and tested. At hot end temperature T_h=33 °C and cold end temperature T_c=30 °C, the actual maximum P_{out} of TEG is about 0.2 mW, and the actual maximum P_{out} of TEG module is about 1.602 mW, which is highly consistent with the simulated value. This work brings great convenience to research and development of wearable thermoelectric modules and provides new, environmentally friendly and efficient power solution for wearable devices.

Keywords: Wearable thermoelectric generator; Bi_2Te_3; Finite element simulation; Power generation

1. Introduction

With the improvement of people's living standards, wearable devices have become an indispensable part of people's lives, including smart watches, smart glasses, smart bracelets, etc. [1–4]. However, the battery capacity and energy density of wearable devices limit their service life and stability, which has become a major obstacle limiting their development and application [5–8]. Therefore, it has become a global consensus to develop and apply green energy technologies [9,10].

As an emerging green energy technology, thermoelectric (TE) power generation can harvest energy from temperature difference in the environment to drive electronic devices by using Seebeck effect (Figure 1A), which effectively solves the problems such as insufficient battery capacity of traditional wearable devices [11–13]. Thermoelectric generator (TEG) is a solid-state device that contains no mechanical moving parts, thus requiring no maintenance, high reliability, and noiseless operation, while being lightweight, compact, and taking up little space [14–17]. Furthermore, wearable thermoelectric generators (w-TEGs) have been studied by many scholars [18–22].

Preprints (www.preprints.org) | NOT PEER-REVIEWED | Posted: 26 April 2023 doi:10.20944/preprints202304.0967.v1

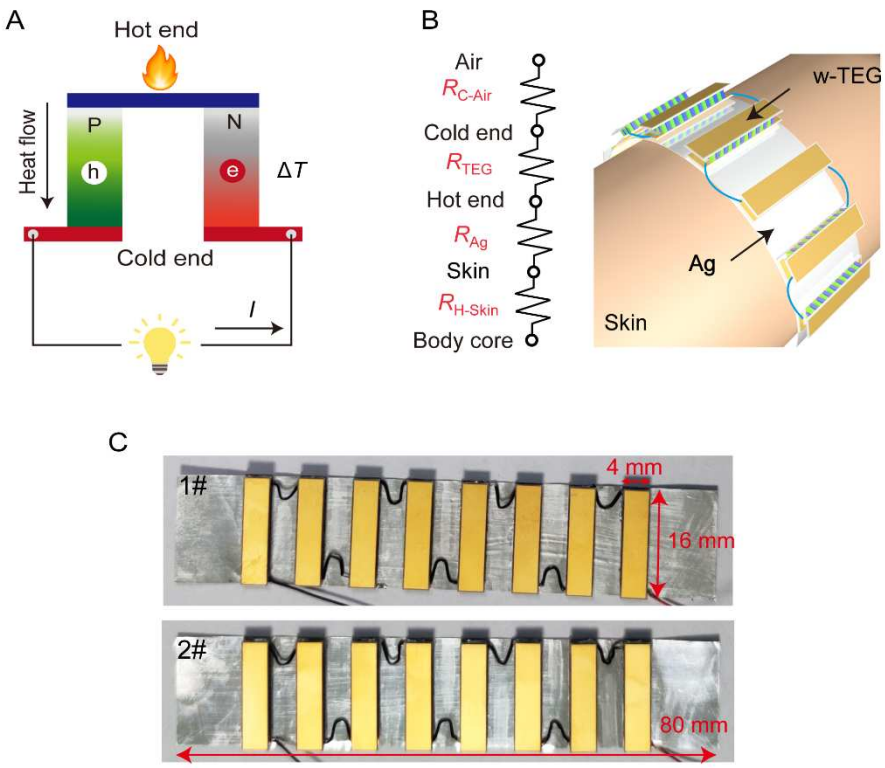

Figure 1. Flexible design of wearable thermoelectric generator. (**A**) schematic diagram of Seebeck effect; (**B**) model of w-TEG on the arm and its equivalent thermal resistance; (**C**) physical image of the w-TEG modules 1# and 2#.

Fan et al. [23] used a simple cutting and gluing method to fabricate a w-TEG containing 48 pairs of P/N thermoelectric cells while without a ceramic substrate. The w-TEG can be well attached to the human body, and the maximum power density of w-TEG was 7.9 μWcm^{-2} and 43.6 μWcm^{-2} under windless and normal walking conditions, respectively. Liu et al. [24] used a radiative cooling coating on the w-TEG. Compared to the original device without the radiation cooling coating, its output power was increased by 128% in an exposed environment and 96% in a non-exposed environment. Its output power density was about 5.5 μWcm^{-2} when the room temperature was 295 K. Zhang et al. [4] prepared a flexible micro-TEG with high power density and light mass by pulse plating technique and effectively reduced the contact resistance between the thermoelectric unit and the electrode by adjusting the plating conditions. The optimized flexible micro-TEG has a maximum area power density and mass power density as high as 14.3 mWcm^{-2} and 189 mWg^{-1}, respectively, at a temperature difference of 29.9 °C. Liang et al. [6] designed a non-planar π-type flexible TEG with passive radiation cooling and a wave-shaped heat sink instead of metal heat sink. The output power density of 12.36 μWcm^{-2} and voltage density of 4.04 mVcm^{-2} at 23 °C when worn on the human body is sufficient to drive some microwatt or sub-microwatt wearable electronics.

W-TEGs can be flexible using three approaches: fabrication of thin-film type TEGs, TEGs using conductive polymers as thermoelectric units, and TEGs using flexible organic substrates connected to rigid inorganic thermoelectric units [25–31]. However, thin-film type thermoelectric units have difficulty in establishing a large enough temperature difference and their power generation performance is usually poor [32–35]. Although conductive polymers are flexible thus to fit the skin well, their low power factor largely limits the power generation performance of the corresponding TEG [36–39]. While the TE properties of inorganic semiconductors are excellent, and by using flexible connections, the resulting TEGs not only have high P_{out} but also good flexibility [40–44]. By using rigid thermoelectric cells in the flexible design of the "strap", such a TEG can generate enough power and still fit well on the humanbody.

Preprints (www.preprints.org) | NOT PEER-REVIEWED | Posted: 26 April 2023 doi:10.20944/preprints202304.0967.v1

In the current context of environmental pollution and energy shortage, the research and application of w-TEGs is of great significance [45–49]. This study aims to improve the power generation performance of thermoelectric devices in the wearable scenario. The device structure is optimized by finite element simulation, and the overall wearability of the module is achieved by the "rigid device-flexible connection" approach. The effect of convective heat transfer coefficient h on the effective temperature difference of the device in a typical wearable scenario is explored, and the TE leg length L is optimized. This study shows the direction for the performance optimization of Bi_2Te_3-based thermoelectric modules in wearable scenarios.

2. Experimental

2.1. Finite Element Modeling

In different environments, the human body maintains a stable temperature through its thermoregulatory system. This process involves changes in thermal resistance of human skin [50]. In this study, we used a simplified human thermoregulation model for finite element simulation and introduced virtual thermal resistance to represent heat transfer properties in the skin. When the ambient temperature is lower than 25 °C, the thermal resistance of skin remains constant; however, when the ambient temperature exceeds 25 °C, thermal resistance suddenly decreases [51–53].

The model consists of three parts: skin, flexible substrate, and thermoelectric devices. The equivalent thermal resistance of these parts is shown in Figure 1B and the finite element model is shown in Figure S1. In this paper, we adopt the "rigid device-flexible connection" approach. Specifically, we connect eight thermoelectric devices with equal size of 16×4 mm^2 in series to form a module and solder them on a silver foil to realize the flexible design (Figure 1B). The thermoelectric materials are p-type $Bi_{0.5}Sb_{1.5}Te_3$ and n-type $Bi_2Te_{2.7}Se_{0.3}$ (Table S1). The electrode and substrate materials are Cu and AlN ceramics, respectively, and the solder is an Au-Sn alloy. The thermal conductivity and resistivity of these materials are shown in Table S2. All simulations in this study were performed using ANSYS Workbench finite element software, and each process was repeated until convergence.

2.2. Boundary Conditions Setting

The corresponding thermodynamic relationships of heat flux and current density are as follows:

$$\nabla(\kappa\nabla T) + \frac{\boldsymbol{J}^2}{\sigma} - T\boldsymbol{J}\cdot\left[\left(\frac{\partial\alpha}{\partial T}\right)\nabla T + (\nabla\alpha)_T\right] = 0 \quad (1)$$

$$\nabla\cdot\boldsymbol{J} = 0 \quad (2)$$

$$\boldsymbol{J} = -\sigma(\nabla V + \alpha\nabla T) \quad (3)$$

$$\boldsymbol{q} = \alpha T\boldsymbol{J} - \kappa\nabla T \quad (4)$$

where the Seebeck coefficient (α), thermal conductivity (κ), electrical conductivity (σ) are the intrinsic properties of TE materials, T is the absolute temperature, V is the electrostatic potential. The vectors $\boldsymbol{J}$ and $\boldsymbol{q}$ represent the current density and heat flux density, respectively.

To refine the model and simplify calculations, the following reasonable assumptions are proposed:

(1) All surfaces (except the hot and cold ends) are considered to be well thermally insulated;

(2) The simulation does not consider the heat sink (if any) and its effects are considered in thermal boundary conditions.

(3) The electric contact resistance (R_{ec}) and thermal contact resistance (R_{tc}) between electrodes and TE legs are both taken into account in the finite element model (Figure S2), which are set to 3.0 $\mu\Omega\cdot cm^2$ and 1×10^{-5} m^2K/W. The other interfacial contact thermal resistances are neglected.

(4) The nonlinear temperature dependence of α, κ, σ are considered.

(5) Thomson effect is neglected.

Preprints (www.preprints.org) | NOT PEER-REVIEWED | Posted: 26 April 2023 doi:10.20944/preprints202304.0967.v1

2.3. w-TEG Module Fabricating

According to the designed connection circuit, copper electrodes (0.025 mm) were patterned on the AlN substrate (0.25 mm) by an adhesive-free calendering method. The copper electrode surface was gold-plated to improve welding reliability and thus reduce the R_{ec}. p-type $Bi_{0.5}Sb_{1.5}Te_3$ and n-type $Bi_2Te_{2.7}Se_{0.3}$ bulk materials were cut into cuboid-shaped legs, of which the upper and lower surfaces were pre-plated with nickel (~5 μm) and gold (~100 nm) film. Then, the sandwich structure composed of "AlN substrate/TE legs/AlN substrate" was welded together by AuSn solder to make micro thermoelectric devices. The module is formed by connecting eight thermoelectric devices in series with copper wires and soldering them to a 0.1 mm thick silver foil using AuSn solder to achieve a "rigid device-flexible connection" as shown in Figure 1C. The detailed preparation process can also be checked in our previous article [5,8,17,53].

3. Results and Discussion

3.1. Effective Temperature Difference of TEG under Different Convective Heat Transfer Coefficients

Figure 2 shows the temperature field of the TE devices with convective heat transfer coefficients on the cold end of 5, 50, 100 and 200 W/(m²°C), respectively. When the ambient temperature T_{air} is 25 °C, the maximum device temperature T_{max} is 37 °C, while the minimum device temperature T_{min} decreases with the increase of convective heat transfer coefficient. In a typical wearable scenario, the natural convection heat transfer coefficient of air is 5 W/(m² °C), and the minimum temperature T_{min} of the device is 36.899 °C at this time, and the average temperature difference ΔT is 0.1 °C. In the case of forced convection heat transfer, the air convection heat transfer coefficient is 50 W/(m² °C), and the minimum temperature T_{min} of the device is 36.06 °C, and the average temperature difference ΔT is 0.94 °C. When the convective heat transfer coefficient increases to 50 W/(m² °C), the minimum temperature T_{min} of the device is 35.255 °C and the average temperature difference ΔT is 1.75 °C. When the convective heat transfer coefficient increases to 200 W/(m² °C), the minimum device temperature T_{min} is 33.946 °C and the average temperature difference ΔT is 3.05 °C.

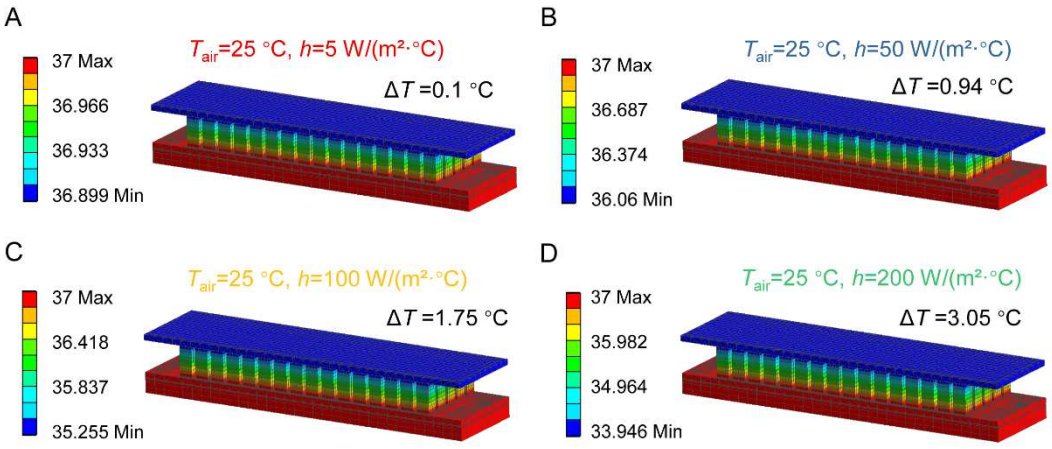

Figure 2. Temperature field of TEG with different convective heat transfer coefficients on the cold end. (**A**) h=5 W/(m²·°C); (**B**) h=50 W/(m²·°C); (**C**) h=100 W/(m²·°C); (**D**) h=200 W/(m²·°C).

As shown in Figure 2, increasing convective heat transfer coefficient h at cold end leads to an increase in temperature difference between two ends of device which provides guidance for optimizing power generation performance of device in wearable scenario.

Preprints (www.preprints.org) | NOT PEER-REVIEWED | Posted: 26 April 2023 doi:10.20944/preprints202304.0967.v1

3.2. Power Generation Performance Optimization of TEG under Different Convective Heat Transfer Coefficients

Figure 3 shows the P_{out} and U_{oc} of a TEG with different leg lengths under h = 5, 50, 100 and 200 W/(m² °C) on the cold-end. The results show that the maximum P_{out} increases and then decreases as the current increases. Both the maximum P_{out} and U_{oc} increase gradually with the increase of h and TE leg length.

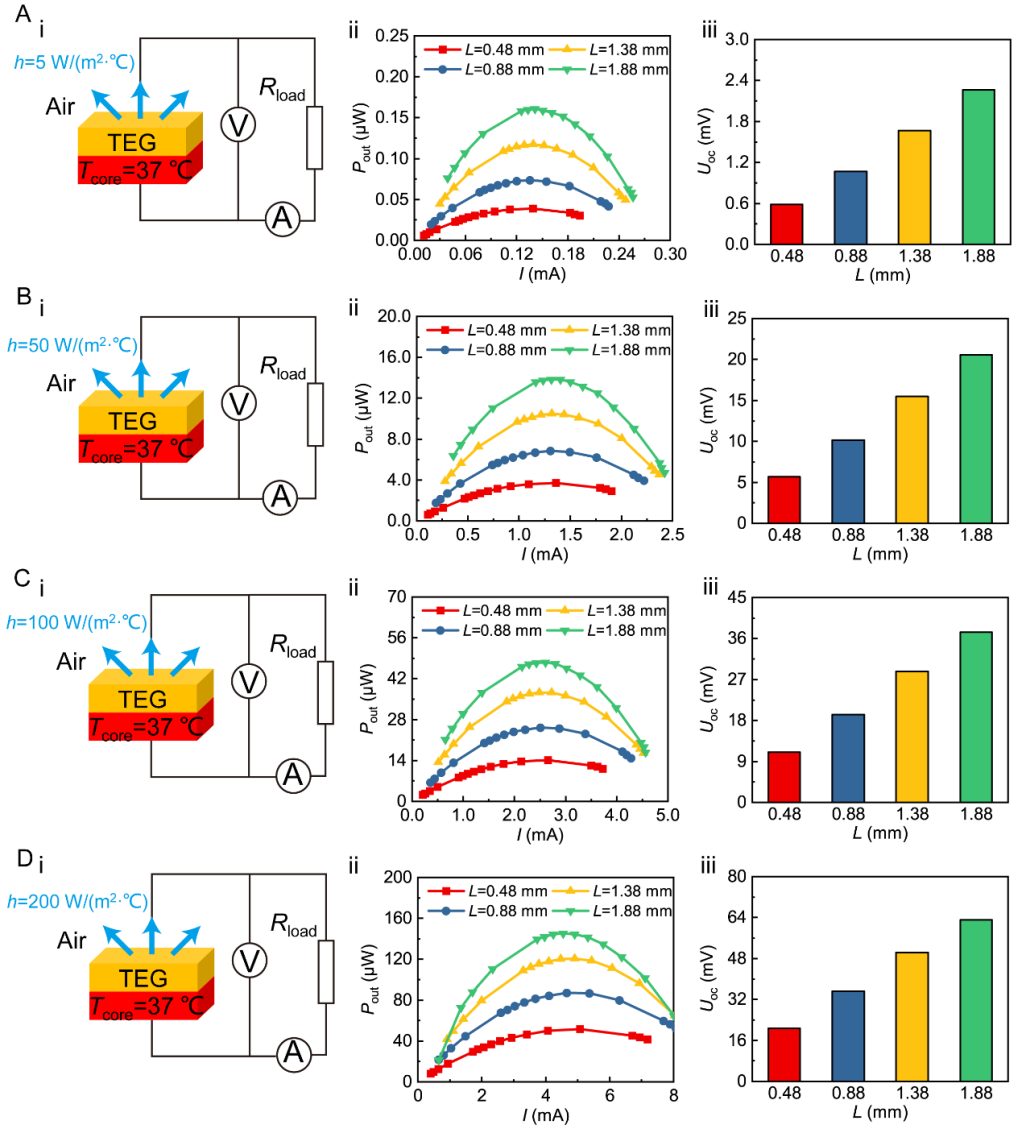

Figure 3. Open circuit voltage and output power of TEG with different convective heat transfer coefficients on the cold end: (**A**) h =5 W/(m² °C); (**B**) h =50 W/(m² °C); (**C**) h =100 W/(m² °C); (**D**) h =200 W/(m² °C).

At h=5 W/(m² °C), the maximum P_{out} of the TEGs with leg length L of 0.48 mm, 0.88 mm, 1.38 mm, and 1.88 mm are 0.039 μW, 0.074 μW, 0.117 μW, and 0.161 μW, and the U_{oc} of the TEGs are 0.583 mV, 1.07 mV, 1.67 mV and 2.26 mV, respectively (Figure 3A). The maximum P_{out} and U_{oc} of the TEG with a leg length of 1.88 mm are 4.1 and 3.9 times higher than those of the L=0.48 mm TEG, respectively.

As the convective heat transfer coefficient h increases to 50 W/(m² °C), the maximum output power P_{out} of the four TEGs are 3.71 μW, 6.85 μW, 10.5 μW, and 13.8 μW, and the open-circuit voltage U_{oc} of the devices are 5.67 mV, 10.2 mV, 15.5 mV, and 20.6 mV (Figure 3B), respectively. The P_{out} and U_{oc} of TEG with the longest TE leg are both about 3~4 times higher than those with the shortest TE

Preprints (www.preprints.org) | NOT PEER-REVIEWED | Posted: 26 April 2023 doi:10.20944/preprints202304.0967.v1

leg. As the h increases to 100 W/(m² °C), the maximum P_{out} of the TEGs is about 300 times higher than that at h=5 W/(m² °C) (Figure 3C). The U_{oc} of the TEGs are 16~19 times higher than that at h=5 W/(m² °C). As h increases to 200 W/(m² °C) (Figure 3D), the maximum P_{out} of the TEGs is 900~1300 times higher than that at h=5 W/(m² °C) (Figure 3D). The U_{oc} of the TEGs are about 30 times higher than that at h=5 W/(m² °C), respectively.

It can be obviously seen from Figure 3 that for TEGs with any leg length, the larger the h, the better the heat dissipation effect and the better the power generation performance of the device. For the same cold-end convective heat transfer coefficient h, the longer the TE leg length L, the larger the effective temperature difference between the two ends of the device, and the larger output power and open-circuit voltage of the device.

However, as h increases, increasing L to optimize device power generation performance gradually becomes less effective. Therefore, in wearable scenarios, it is necessary to design a reasonable heat dissipation structure and select efficient heat dissipation materials to improve h at the cold end of the device. This will improve the ΔT_{eff} and power generation performance of the device.

3.3. Power Generation Performance Optimization of TEG under Fixed Temeprature Difference Conditions

According to the results in Section 3.1, the ΔT_{eff} between the two ends of TEG ranges from 0.1 °C to 3.05 °C in a typical wearable scenario. Therefore, it is necessary to investigate how to optimize device power generation performance under fixed temperature difference conditions.

Figure 4 shows the P_{out} and U_{oc} of TEGs with different TE legs under a temperature difference ΔT of 1 and 3 °C. It is observed that the P_{out} increases and then decreases with the increase of current under these two different temperature differences, and the maximum P_{out} and U_{oc} increase gradually with temperature difference. It should be noted, however, that the maximum P_{out} decreases with increasing TE leg length.

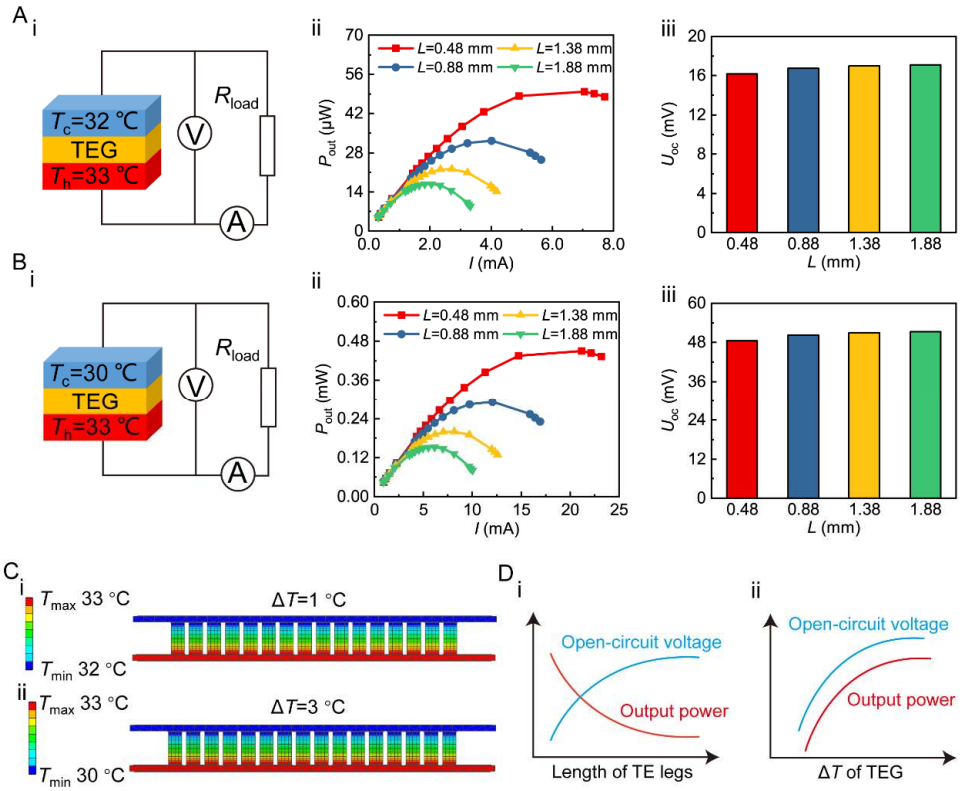

Figure 4. Optimization of the power generation performance of TEG under fixed temperature difference conditions. Open circuit voltage and output power: (**A**) at ΔT=1°C, (**B**) at ΔT=3°C; (**C**) temperature field of TEG; (**D**) relationship between P_{out} and U_{oc} and TE legs length and ΔT.

Preprints (www.preprints.org) | NOT PEER-REVIEWED | Posted: 26 April 2023 doi:10.20944/preprints202304.0967.v1

At ΔT=1 °C, the maximum P_{out} of devices with TE leg length L of 0.48 mm, 0.88 mm, 1.38 mm, and 1.88 mm are 49.9 μW, 32.3 μW, 22.2 μW, and 16.8 μW, and the U_{oc} is 16.2 mV, 16.7 mV, 17.0 mV, and 17.1 mV, respectively (Figure 4A). The maximum P_{out} of device with TE leg length of 1.88 mm is 66.3% lower than that of L=0.48 mm device. Meanwhile, the U_{oc} increases by 5.6%.

As ΔT increases to 3 °C, the maximum P_{out} of four TEGs with different TE leg lengths are 0.451 mW, 0.292 mW, 0.200 mW, and 0.152 mW; the U_{oc} are 48.5 mV, 50.2 mV, 50.9 mV, and 51.3 mV respectively (Figure 4B). When the hot end temperature T_h is 33 °C and cold end temperature T_c is 32 °C and 30 °C, the temperature field of the TEG can be displayed in Figure 4C.

According to Figure 4D, the TEG resistance gradually increases with increase of TE leg length under a fixed temperature difference between two ends (Figure S3); and the P_{out} gradually decreases but the U_{oc} slightly increases. In addition, the Seebeck effect of material is enhanced as temperature difference between two ends increases, thus improving power generation performance of device.

3.4. Power Generation Performance Verification of TEG Module under Different Temeprature Differences

Figure 5A shows the schematic and physical diagram of self- designed test system for power generation performance of TEG. The system consists of temperature-controlled platform, data collector, load resistor, and computer. w-TEG to be tested is placed between two temperature-controlled platforms. By adjusting spring-loaded knobs and applying thermal grease to contact surfaces, w-TEG is in close contact with upper and lower temperature-controlled platforms to improve heat utilization. w-TEG is connected and driven by loads with different resistances. Data collector records the output voltage V and current I, then the output power is calculated by P=VI. All test is done in vacuum chamber.

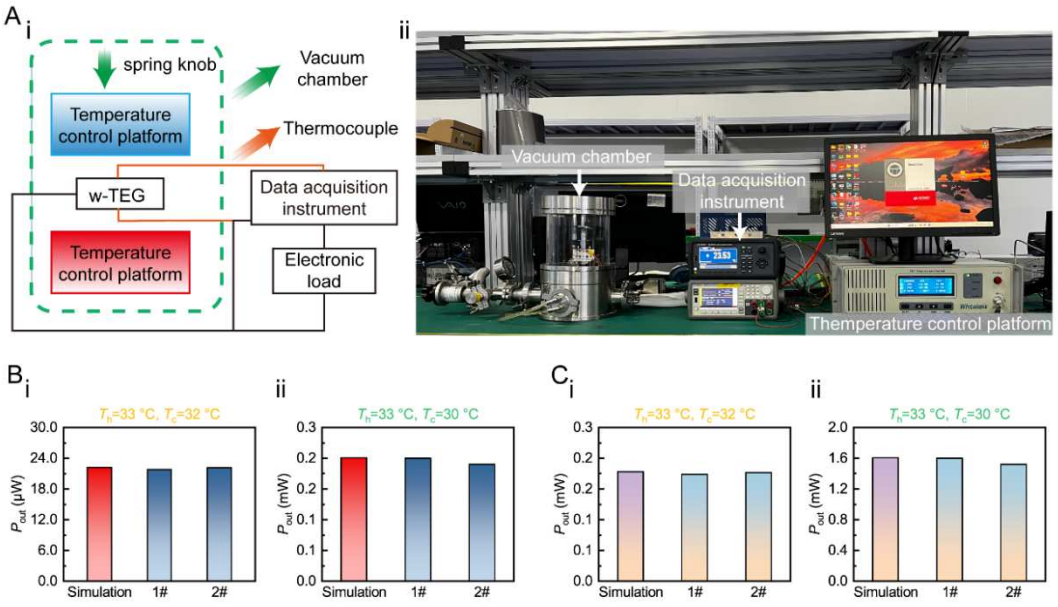

Figure 5. Power generation performance testing of TEG and its w-TEG module. (**A**) schematic and physical diagram of the self-designed test system; (**B**) output power of TEGs; (**C**) output power of w-TEG modules.

From Sections 3.1 and 3.2, it can be seen that longer length of TE leg leads to better power generation performance of TEG in typical wearable scenario. However, from industrial processing experience, the ratio of TE leg length to width, i.e., L/W, should not exceed 3; otherwise, TE leg will easily fracture and fail.

To verify power generation performance of thermoelectric devices in accordance with simulated results, sixteen 16×4×2 mm² TEGs (L=1.38 mm, W=0.6 mm) and two modules were fabricated and tested. At hot end temperature of T_h=33 °C and cold end temperature of T_c=32 °C, the actual maximum

P_{out} of 1# and 2# TEGs are 21.8 μW and 22.1 μW, respectively (Figure 5B$_i$), and the actual maximum P_{out} of 1# and 2# TEG modules are 0.174 mW and 0.177 mW, respectively (Figure 5B$_{ii}$). Compared with the simulated value, the difference is only 2.3% and 0.6%. At hot end temperature T_h=33 °C and cold end temperature T_c=30 °C, the actual maximum P_{out} of 1# and 2# TEGs are 0.2 mW and 0.19 mW, respectively (Figure 5C$_i$), and the actual maximum P_{out} of 1# and 2# TEG modules are 1.602 mW and 1.52 mW, respectively (Figure 5C$_{ii}$), which is only 0.4% different from simulated value. The above experimental results show that finite element simulation successfully guides design of w-TEG.

4. Conclusions

Through finite element simulation, this study successfully designed high-performance thermoelectric generator (TEG) and made it into wearable thermoelectric module by adopting "rigid device-flexible connection" method. It was found that in typical wearable scenario, higher convective heat transfer coefficient (h) on cold-end leads to larger effective temperature difference (ΔT_{eff}) and better power generation performance of device. Meanwhile, at same h on the cold-end, longer TE leg length leads to larger ΔT_{eff} established at both ends of device, larger device output power (P_{out}) and open-circuit voltage (U_{oc}). However, when the h increases to a certain level, optimization effect of increasing TE leg length on device power generation performance will gradually diminish. For devices with fixed temperature difference between two ends, longer TE leg length leads to higher resistance of TEG, resulting in lower P_{out} but slight increase in U_{oc}. Finally, sixteen 16×4×2 mm^2 TEGs (L=1.38 mm, W=0.6 mm) and two modules were fabricated and tested. At hot end temperature T_h=33 °C and cold end temperature T_c=30 °C, the actual maximum P_{out} of TEG is about 0.2 mW, and the actual maximum P_{out} of TEG module is about 1.602 mW, which is highly consistent with the simulated value.

Supplementary Materials: The following supporting information can be downloaded at the website of this paper posted on Preprints.org. Figure S1. Finite element model of w-TEG. Figure S2. TEG unit and its internal structure. Figure S3. Resistance of TEG with different thermoelectric leg lengths. Table S1. Thermoelectric material properties in the temperature range 303 to 333K. Table S2. Material properties used in the simulation.

Author Contributions: D.Y. and Y.Y. conceived the project; Y.X. (Yubing Xing), K.T. and Y.L. carried out the finite element simulation; Y.X. (Yubing Xing), D.Y., K.H., J.W., Y.X. (Yani Xiao), J.L. (Jianan Lyu) and J.L. (Junhao Li) prepared the TEGs and tested their output power generation performance; Y.X. (Yubing Xing), D.Y., P.Z. and Y.Y. analyzed the experimental data; Y.X. and D.Y. co-wrote the manuscript. All authors have read and agreed to the published version of the manuscript.

Acknowledgments: This work was financially supported by the National Natural Science Foundation of China (52202289), the International Postdoctoral Exchange Fellowship Program (PC2022044), and the National Key Research and Development Program of China (2019YFA0704900).

Conflicts of Interest: The authors declare no competing financial interest.

References

1. Yu, Y. et al. Wearable Respiration Sensor for Continuous Healthcare Monitoring Using a Micro-Thermoelectric Generator with Rapid Response Time and Chip-Level Design. *Advanced Materials Technologies* **7**, doi:10.1002/admt.202101416 (2022).
2. Zou, Q. et al. Bi2Te3-based flexible thermoelectric generator for wearable electronics. *Applied Physics Letters* **120**, doi:10.1063/5.0078389 (2022).
3. Fan, W. et al. High-Performance Stretchable Thermoelectric Generator for Self-Powered Wearable Electronics. *Adv Sci (Weinh)*, e2206397, doi:10.1002/advs.202206397 (2023).
4. Zhang, J. et al. Flexible micro thermoelectric generators with high power density and light weight. *Nano Energy* **105**, doi:10.1016/j.nanoen.2022.108023 (2023).
5. Hu, K. et al. Optimized thermal design for excellent wearable thermoelectric generator. *Journal of Materials Chemistry A*, doi:10.1039/d2ta06966k (2022).

6. Liang, J., Huang, M., Zhang, X. & Wan, C. Structural design for wearable self-powered thermoelectric modules with efficient temperature difference utilization and high normalized maximum power density. *Applied Energy* **327**, doi:10.1016/j.apenergy.2022.120067 (2022).
7. Shi, Y. et al. Stretchable thermoelectric generator for wearable power source and temperature detection applications. *Energy Conversion and Management* **253**, doi:10.1016/j.enconman.2021.115167 (2022).
8. You, H. et al. Flexible Bi2Te3-based thermoelectric generator with an ultra-high power density. *Applied Thermal Engineering* **202**, doi:10.1016/j.applthermaleng.2021.117818 (2022).
9. Hasan, M. N., Nayan, N., Nafea, M., Muthalif, A. G. A. & Mohamed Ali, M. S. Novel structural design of wearable thermoelectric generator with vertically oriented thermoelements. *Energy* **259**, doi:10.1016/j.energy.2022.125032 (2022).
10. He, X. et al. Continuous manufacture of stretchable and integratable thermoelectric nanofiber yarn for human body energy harvesting and self-powered motion detection. *Chemical Engineering Journal* **450**, doi:10.1016/j.cej.2022.137937 (2022).
11. He, W. et al. Recent development and application of thermoelectric generator and cooler. *Applied Energy* **143**, 1-25, doi:10.1016/j.apenergy.2014.12.075 (2015).
12. Twaha, S., Zhu, J., Yan, Y. & Li, B. A comprehensive review of thermoelectric technology: Materials, applications, modelling and performance improvement. *Renewable and Sustainable Energy Reviews* **65**, 698-726, doi:10.1016/j.rser.2016.07.034 (2016).
13. Champier, D. Thermoelectric generators: A review of applications. *Energy Conversion and Management* **140**, 167-181, doi:10.1016/j.enconman.2017.02.070 (2017).
14. Zhang, T. Design and optimization considerations for thermoelectric devices. *Energy Conversion and Management* **112**, 404-412, doi:10.1016/j.enconman.2016.01.033 (2016).
15. Nozariasbmarz, A. et al. Review of wearable thermoelectric energy harvesting: From body temperature to electronic systems. *Applied Energy* **258**, doi:10.1016/j.apenergy.2019.114069 (2020).
16. Hasan, M. N., Nafea, M., Nayan, N. & Mohamed Ali, M. S. Thermoelectric Generator: Materials and Applications in Wearable Health Monitoring Sensors and Internet of Things Devices. *Advanced Materials Technologies* **7**, doi:10.1002/admt.202101203 (2021).
17. Yuan, X. et al. Bi2Te3-based wearable thermoelectric generator with high power density: from structure design to application. *Journal of Materials Chemistry C* **10**, 6456-6463, doi:10.1039/d2tc00426g (2022).
18. Yan, Q. & Kanatzidis, M. G. High-performance thermoelectrics and challenges for practical devices. *Nat Mater*, doi:10.1038/s41563-021-01109-w (2021).
19. Park, K. T. et al. Highly Integrated, Wearable Carbon-Nanotube-Yarn-Based Thermoelectric Generators Achieved by Selective Inkjet-Printed Chemical Doping. *Advanced Energy Materials* **12**, doi:10.1002/aenm.202200256 (2022).
20. Li, Y., Shi, Y., Wang, X., Luo, D. & Yan, Y. Thermal and electrical contact resistances of thermoelectric generator: Experimental study and artificial neural network modelling. *Applied Thermal Engineering* **225**, doi:10.1016/j.applthermaleng.2023.120154 (2023).
21. Pan, H. & Zhao, D. An improved model for performance predicting and optimization of wearable thermoelectric generators with radiative cooling. *Energy Conversion and Management* **284**, doi:10.1016/j.enconman.2023.116981 (2023).
22. Wu, B. et al. Stretchable thermoelectric generators with enhanced output by infrared reflection for wearable application. *Chemical Engineering Journal* **453**, doi:10.1016/j.cej.2022.139749 (2023).
23. Fan, W. et al. High-Power-Density Wearable Thermoelectric Generators for Human Body Heat Harvesting. *ACS Appl Mater Interfaces* **14**, 21224-21231, doi:10.1021/acsami.2c03431 (2022).
24. Liu, Y. et al. Passive Radiative Cooling Enables Improved Performance in Wearable Thermoelectric Generators. *Small* **18**, e2106875, doi:10.1002/smll.202106875 (2022).
25. Mytafides, C. K., Tzounis, L., Karalis, G., Formanek, P. & Paipetis, A. S. High-Power All-Carbon Fully Printed and Wearable SWCNT-Based Organic Thermoelectric Generator. *ACS Appl Mater Interfaces* **13**, 11151-11165, doi:10.1021/acsami.1c00414 (2021).
26. Zheng, Y. et al. Durable, stretchable and washable inorganic-based woven thermoelectric textiles for power generation and solid-state cooling. *Energy & Environmental Science* **15**, 2374-2385, doi:10.1039/d1ee03633e (2022).
27. Chen, K. et al. Flexible Thermoelectrics Based on Plastic Inorganic Semiconductors. *Advanced Materials Technologies*, doi:10.1002/admt.202300189 (2023).

28. Shen, Y. et al. Review on Fiber-Based Thermoelectrics: Materials, Devices, and Textiles. *Advanced Fiber Materials*, doi:10.1007/s42765-023-00267-7 (2023).
29. Tian, Y. et al. Optimizing the output performance and parasitic depletion of Bi2Te3-based thermoelectric generators by using a high-density approach. *Journal of Materials Chemistry A*, doi:10.1039/d3ta01342a (2023).
30. Wu, M. et al. High Thermoelectric Performance and Ultrahigh Flexibility Ag(2)S(1-x)Se(x) film on a Nylon Membrane. *ACS Appl Mater Interfaces* **15**, 8415-8423, doi:10.1021/acsami.2c21987 (2023).
31. Zhu, P. et al. A self-healable, recyclable, and flexible thermoelectric device for wearable energy harvesting and personal thermal management. *Energy Conversion and Management* **285**, doi:10.1016/j.enconman.2023.117017 (2023).
32. Newbrook, D. W. et al. Mathematical model and optimization of a thin-film thermoelectric generator. *Journal of Physics: Energy* **2**, doi:10.1088/2515-7655/ab4242 (2019).
33. Liang, L. et al. Initiating a Stretchable, Compressible, and Wearable Thermoelectric Generator by a Spiral Architecture with Ternary Nanocomposites for Efficient Heat Harvesting. *Advanced Functional Materials* **32**, doi:10.1002/adfm.202111435 (2021).
34. Soleimani, Z., Zoras, S., Ceranic, B., Cui, Y. & Shahzad, S. A comprehensive review on the output voltage/power of wearable thermoelectric generators concerning their geometry and thermoelectric materials. *Nano Energy* **89**, doi:10.1016/j.nanoen.2021.106325 (2021).
35. Chen, C. et al. Structural Design of Nanowire Wearable Stretchable Thermoelectric Generator. *Nano Lett* **22**, 4131-4136, doi:10.1021/acs.nanolett.2c00872 (2022).
36. Liao, Z. et al. Intrinsically Self-Healable and Wearable All-Organic Thermoelectric Composite with High Electrical Conductivity for Heat Harvesting. *ACS Appl Mater Interfaces* **14**, 43421-43430, doi:10.1021/acsami.2c13593 (2022).
37. Sun, T., Wang, L. & Jiang, W. Pushing thermoelectric generators toward energy harvesting from the human body: Challenges and strategies. *Materials Today* **57**, 121-145, doi:10.1016/j.mattod.2022.06.001 (2022).
38. Wu, Z., Zhang, S., Liu, Z., Mu, E. & Hu, Z. Thermoelectric converter: Strategies from materials to device application. *Nano Energy* **91**, doi:10.1016/j.nanoen.2021.106692 (2022).
39. Zhang, Y. et al. Novel Wearable Pyrothermoelectric Hybrid Generator for Solar Energy Harvesting. *ACS Appl Mater Interfaces* **14**, 17330-17339, doi:10.1021/acsami.2c00874 (2022).
40. Shittu, S., Li, G., Zhao, X. & Ma, X. Review of thermoelectric geometry and structure optimization for performance enhancement. *Applied Energy* **268**, doi:10.1016/j.apenergy.2020.115075 (2020).
41. Han, Y., Simonsen, L. E. & Malakooti, M. H. Printing Liquid Metal Elastomer Composites for High-Performance Stretchable Thermoelectric Generators. *Advanced Energy Materials* **12**, doi:10.1002/aenm.202201413 (2022).
42. Kim, W.-G., Kim, D., Lee, H. M. & Choi, Y.-K. Wearable fabric-based hybrid energy harvester from body motion and body heat. *Nano Energy* **100**, doi:10.1016/j.nanoen.2022.107485 (2022).
43. Kuang, N. et al. High performance flexible thermoelectric generator using bulk legs and integrated electrodes for human energy harvesting. *Energy Conversion and Management* **272**, doi:10.1016/j.enconman.2022.116337 (2022).
44. Lv, J.-R., Ma, J.-L., Dai, L., Yin, T. & He, Z.-Z. A high-performance wearable thermoelectric generator with comprehensive optimization of thermal resistance and voltage boosting conversion. *Applied Energy* **312**, doi:10.1016/j.apenergy.2022.118696 (2022).
45. Cui, Y. J., Wang, B. L. & Wang, K. F. Energy conversion performance optimization and strength evaluation of a wearable thermoelectric generator made of a thermoelectric layer on a flexible substrate. *Energy* **229**, doi:10.1016/j.energy.2021.120694 (2021).
46. Zhang, Q., Deng, K., Wilkens, L., Reith, H. & Nielsch, K. Micro-thermoelectric devices. *Nature Electronics* **5**, 333-347, doi:10.1038/s41928-022-00776-0 (2022).
47. Pei, Q.-X., Guo, J.-Y., Suwardi, A. & Zhang, G. Insights into interfacial thermal conductance in Bi2Te3-based systems for thermoelectrics. *Materials Today Physics* **30**, doi:10.1016/j.mtphys.2022.100953 (2023).
48. Zhu, S. et al. Persistently self-powered wearable thermoelectric generator enabled by phase-change inorganics as the heat sink. *Materials Today Physics* **32**, doi:10.1016/j.mtphys.2023.101011 (2023).
49. Zuo, Q. et al. Performance analysis of thermoelectric generator system in different aspect ratio collector channels. *Applied Thermal Engineering* **226**, doi:10.1016/j.applthermaleng.2023.120330 (2023).
50. Zhang, A., Pang, D., Wang, B. & Wang, J. Dynamic responses of wearable thermoelectric generators used for skin waste heat harvesting. *Energy* **262**, doi:10.1016/j.energy.2022.125621 (2023).

51. Suarez, F., Nozariasbmarz, A., Vashaee, D. & Öztürk, M. C. Designing thermoelectric generators for self-powered wearable electronics. *Energy & Environmental Science* **9**, 2099-2113, doi:10.1039/c6ee00456c (2016).
52. Wijethunge, D., Kim, D. & Kim, W. Simplified human thermoregulatory model for designing wearable thermoelectric devices. *Journal of Physics D: Applied Physics* **51**, doi:10.1088/1361-6463/aaa17e (2018).
53. Tang, K. et al. Multi-factor roadmap for designing wearable micro thermoelectric generators. *Energy Conversion and Management* **280**, doi:10.1016/j.enconman.2023.116819 (2023).